THE JOURNAL OF PHYSICAL CHEMISTRY C
A JOURNAL OF THE AMERICAN CHEMICAL SOCIETY

pubs.acs.org/JPCC

Article

Molten Salt Synthesis of Persistent Luminescent/Magnetic Cr^{3+}-Doped Zinc Gallogermanate Particles

Published as part of The Journal of Physical Chemistry virtual special issue "Early-Career and Emerging Researchers in Physical Chemistry Volume 2".

Xiaojun Wei, Haoran Ning, Xiaodan Huang, Collin F. Perkinson, Chunyan Liu, Zhuoyao Dong, Lihong Jing,* and Mingyuan Gao*

Cite This: *J. Phys. Chem. C* 2023, 127, 3733−3741

Read Online

ACCESS | Metrics & More | Article Recommendations | Supporting Information

ABSTRACT: Near-infrared persistent luminescent particles are appealing materials for a diverse range of optoelectronic and biomedical applications. Thermal treatment at high temperature (e.g., solid-state annealing process) has been shown to enhance the luminescence intensity of these particles, while it remains a challenge to manipulate the morphology and solution dispersibility. Herein, molten salt *in situ* synthesis of Cr^{3+}-doped zinc gallogermanate (ZGGO) with well-defined morphology and solution dispersibility is developed in combination with citric acid. In the absence of the physical grinding treatment (e.g., mechanically milling), the resulting ZGGO particles are not only readily dispersible in the aqueous solution but also exhibit enhanced persistent luminescence. The synergetic effects of salt and citric acid on the particle formation process as well as the optical properties are elucidated. Interestingly, these particles also exhibit enhanced ferromagnetism properties, showing promise for multiple optical/magnetic applications. The molten salt synthesis approach demonstrated in this work offers an alternative pathway for producing persistent luminescent particles, and the method may help to improve the synthesis of other complex metal oxide particles.

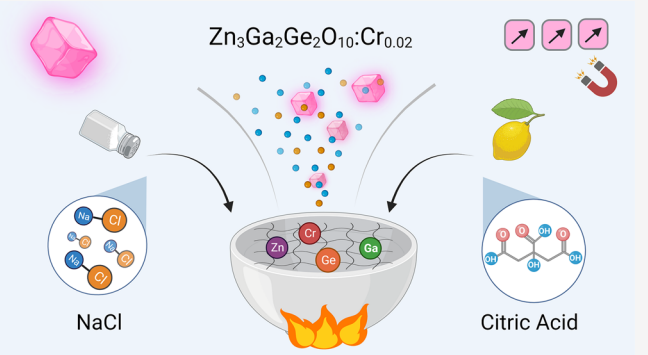

INTRODUCTION

Cr^{3+}-doped gallate phosphors with near-infrared (NIR) persistent luminescence (or afterglow) have attracted scientific interest due to their capability of emitting light long after ceasing optical excitation.[1−5] Persistent luminescence particles have been shown to have utility in a wide range of applications,[4,6−8] including bioimaging/biosensing,[9−11] information storage,[12] signaling technology,[13,14] emergency route signage, and identification markers.[15] Over the past decade, significant progress has been achieved in developing robust synthesis protocols for luminescent particles based on zinc gallate and zinc gallogermanate, with synthetic control of their composition, size, shape, and surface properties.[7,16−21] Currently, high-temperature calcination (~1000 °C) is often relied upon as the most direct and effective approach for improving the optical performance of these materials.[22,23] However, calcination often results in particle aggregation, and the optical properties (e.g., luminescence intensity, afterglow lifetimes, etc.) suffer from weakening due to the mechanically broken facets during post milling/grinding for achieving appropriate particle sizes.[9,24] It is believed that monodisperse crystals have less scattering of excited and emitted photons, favoring persistent luminescence output by d-d transitions of the Cr^{3+} ion from $Zn_3Ga_2Ge_2O_{10}:Cr^{3+}$ (ZGGO) particles.[25] Therefore, avoiding aggregation of the resulting persistent luminescent materials during thermal treatment is of utmost importance for ZGGO particles in order to improve their optical properties and dispersibility in the solution.

To this end, several synthetic modifications have been attempted to avoid aggregation and heterogeneity of ZGGO and $ZnGa_2O_4:Cr^{3+}$ (ZGO) particles.[26−28] Among the existing strategies, SiO_2 is a commonly used material to prevent particle aggregation during the annealing process, owing to its stability under heating and optical excitation. It can act as a reaction site for template synthesis of particles, or the preformed particles can be incorporated into the pores of mesoporous SiO_2 prior to calcination. Nevertheless, harsh conditions used to

Received: November 16, 2022
Revised: January 25, 2023
Published: February 8, 2023

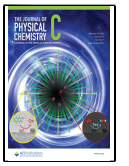

https://doi.org/10.1021/acs.jpcc.2c08045
J. Phys. Chem. C 2023, 127, 3733−3741

subsequently etch the SiO_2 shell often negatively affect the optical properties of particles.[28] From a synthetic point of view, template-free direct synthesis is preferable. Recently, a method based on molten salt assisted annealing of preformed ZGO colloidal particles was introduced, where the persistent luminescence intensity and decay lifetime of ZGO particles were improved while maintaining the initial particle size regime during thermal treatment.[25] By using a water-soluble salt, postprocessing conditions became simple, mild, and scalable in comparison with SiO_2 coating procedures.[29,30] That said, the above synthetic strategy is a two-step process, where the molten salt is used in the second step for shielded sintering. In principle, the molten salt serving as a solvent is expected to assist in dissolving solid reactants and solvating ions by strong polarization and rapid movement of reactant species through convection and diffusion, providing a promising *in situ* synthetic strategy for crystals requiring high temperature calcination.[31−33] For these reasons, use of molten salts may aid the synthesis of persistent luminescent particles while allowing control of morphology and solution dispersibility.

Following our previous investigations on persistent luminescent particles,[1,34,35] herein we report a molten salt-assisted chemical synthesis of Cr^{3+}-doped zinc gallogermanate (ZGGO) particles with well-defined morphology and water dispersibility. Compared with the conventional sol−gel strategy that generally requires subsequent high-temperature solid state annealing, our strategy realizes the direct synthesis of water-dispersible and size-controlled ZGGO particles at high temperature, avoiding postetching or grinding processes. It is found that the network structure formed before heating after the introduction of citric acid is the key factor for direct formation of monodisperse ZGGO particles. The effects of molten salt on the persistent luminescent properties of these ZGGO particles are further probed through steady-state and transient spectroscopy. It is further demonstrated that the resulting particles not only possess improved NIR persistent luminescence but also exhibit enhanced ferromagnetism, showing promising implication for optical/magnetic applications.

METHODS

Chemicals. All reagents were directly used as-received, including zinc nitrate hexahydrate ($Zn(NO_3)_2{\cdot}6H_2O$, 98%, Sigma-Aldrich), gallium(III) oxide (Ga_2O_3, ≥99.99%, Sigma-Aldrich), germanium(IV) oxide (GeO_2, ≥99.99%, Sigma-Aldrich), chromium nitrate nanohydrate ($Cr(NO_3)_3{\cdot}9H_2O$, 99%, Sigma-Aldrich), citric acid (≥99.5%, Sigma-Aldrich), sodium chloride (NaCl, 99.0%, Sigma-Aldrich), ammonium hydroxide solution ($NH_3{\cdot}H_2O$, 28% NH_3 in H_2O, Sigma-Aldrich), nitric acid (HNO_3, 69%, Sigma-Aldrich), and hydrochloric acid (HCl, 37%, Sigma-Aldrich). Ultrapure water (18.2 MΩ·cm@25 °C) was obtained through a Milli-Q Plus system and used throughout the preparation.

Preparation of Solutions. The solution of $Zn(NO_3)_2{\cdot}6H_2O$ (0.6 M), $Cr(NO_3)_3{\cdot}9H_2O$ (0.02 M), and citric acid (1 M) was obtained by dissolving these reagents in ultrapure water directly. $Ga(NO_3)_3$ (0.4 M) was obtained by dissolving Ga_2O_3 in a dilute HNO_3 solution while heating. $Ge(OH)_4$ (0.4 M) was obtained by dissolving GeO_2 in dilute $NH_3{\cdot}H_2O$ at room temperature.

Synthesis of ZGGO Particles. The starting material composition of ZGGO was modified from that described in a previous publication,[2] and the aqueous solutions of Zn^{2+}, Ga^{3+}, Ge^{4+}, and Cr^{3+} were mixed according to the chemical formula of $Zn_3Ga_2Ge_2O_{10}{:}Cr_{0.02}$. To the mixture solution, the citric acid solution was slowly added without any precipitation, and the molar ratio of citric acid to total metal ions was maintained at 1.5:1, followed by the addition of HCl to adjust the pH to 5.5. The solution was vigorously stirred at room temperature for 10 min, followed by the addition of 40 g of NaCl. A powder containing NaCl, metal ions, and citric acid was then obtained by rapid rotary evaporation at 60 °C. Subsequently, the solid precursors were moved to a 50 mL crucible and directly treated in air at 1000 °C for 1 h. The heating process is carried out in a high-temperature muffle furnace that is preheated to 1000 °C in advance, where adequate safety protection should be taken when performing this operation, including goggles, high-temperature protective clothing, and a sufficient safety distance. After being cooled by standing in still air at room temperature, the products were collected from the crucible. NaCl was dissolved upon addition of deionized water, and the resultant ZGGO particles embedded in the salt were precipitated, isolated through centrifugation, washed with water and ethanol for three cycles, and finally redispersed in deionized water for further characterization.

Characterization. Transmission electron microscopy (TEM) images and electron diffraction patterns were obtained using a JEM-100CXII electron microscope operating at an accelerating voltage of 100 kV. Particle size was determined using the ImageJ application by averaging at least 150 particles per sample, and for each particle, the largest diametric distance was denoted as the particle size. X-ray photoelectron spectroscopy (XPS) measurements were performed on a multifunctional photoelectron spectrometer (Escalab 250XI). Dynamic light scattering (DLS) measurements and the ζ-potential test were carried out at 25 °C on a Nano ZS machine (Malvern) equipped with a diode (solid state) laser (λ = 633 nm). Powder X-ray diffraction (XRD) patterns of the particle samples were recorded on a Rigaku D/Max-2500 diffractometer under Cu Kα1 radiation (λ = 1.54056 Å). The magnetic properties of the resulting samples were characterized using a vibrating sample magnetometer (VSM, JDM-13, China). Thermogravimetric analysis (TGA) was performed using a NETZSCH TG209F3 thermogravimetric analyzer. The steady-state luminescence spectra, as well as the absolute photoluminescence quantum yield, and persistent luminescence decay curves of samples were recorded and measured using a steady state/transient FLS980 fluorescence spectrometer (Edinburgh Instruments) equipped with an integrating sphere under excitation at a 254 nm wavelength. The persistent luminescence decay curves were normally recorded after excitation for a period of 5 min.

RESULTS AND DISCUSSION

In a typical molten salt synthesis, as schematically shown in Scheme 1, aqueous solutions of Zn^{2+}, Ga^{3+}, Ge^{4+}, and Cr^{3+} are mixed according to the stoichiometry of $Zn_3Ga_2Ge_2O_{10}{:}Cr_{0.02}$. Citric acid is then added, giving rise to a clear viscous solution. A network structure is observed due to the chelating effect between carboxylic acids of citric acid and metal ions. At this stage, an appropriate amount of acidic solution is added to adjust the pH to 5.5, for optimizing the formation of stable metal citrate species and preventing precipitation of individual hydroxide by promoting the cation binding to the citrate.[36,37] Thereafter, NaCl is dissolved in the metal-citrate gel solutions

https://doi.org/10.1021/acs.jpcc.2c08045
J. Phys. Chem. C 2023, 127, 3733−3741

Scheme 1. Schematic Illustration of the Process to Synthesize $Zn_3Ga_2Ge_2O_{10}$:$Cr_{0.02}$ (ZGGO) Particles[a]

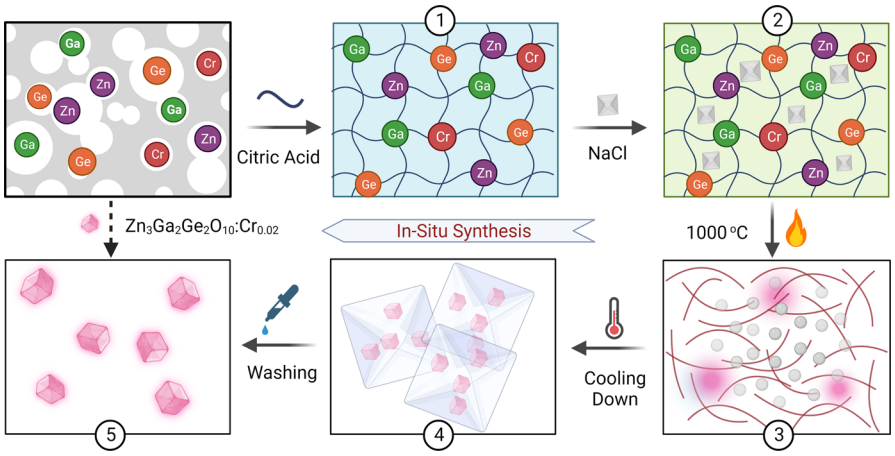

[a]Created with BioRender.com.

and solid powders containing NaCl, metal ions, and citric acid are obtained by rapid rotary evaporation of the gel solution. Subsequently, the solid-state precursor is directly treated at 1000 °C for 1 h (Figure S1, left). Finally, after cooling down to room temperature, the ZGGO particles are obtained by dissolving the solid in water (Figure S1, right). The particle formation mechanism may follow the reactions as presented in Figure S2. In brief, Zn^{2+}, Ga^{3+}, Ge^{4+}, and Cr^{3+} ions react with hydroxyl ions and give rise to metal hydroxides that then form water-soluble complexes upon the complexation of citric acid.[38] Thereafter, these compounds hydrolyze and result in ZGGO particles at high temperature. It is worth mentioning that citric acid is extremely important to stabilize the hydroxide-form precursors, effectively avoiding the precipitation of insoluble metal hydroxides as shown in Figure S3.

Representative transmission electron microscopy (TEM) images (Figure 1a-b) show that the majority of the resulting particles have cube- and quasicube-like shapes though there exist irregular particles, and there is no large-scale particle aggregation. The average size of the ZGGO particles is estimated to be 114.5 ± 31.5 nm (Figure S4), and the relative standard deviation (RSD) as calculated from the corresponding size distribution histogram is 27.5%. The corresponding selected area electron diffraction pattern given in Figure 1c together with the X-ray diffraction (XRD) data in Figure 1d suggests that these particles possess a well-defined cubic spinel phase (cubic space group *Fd3m*) that is characteristic of the bulk $ZnGa_2O_4$ (JCPDS 38-1240) and Zn_2GeO_4 (JCPDS 25-1018) compounds with lattice parameters of a = 8.334 Å and a = 8.350 Å, respectively.[5,23] No peaks from other phases such as ZnO, GeO_2, or Ga_2O_3 appear. In comparison with the XRD pattern of ZGGO without Cr^{3+} dopants, no obvious shift in peak position of $Zn_3Ga_2Ge_2O_{10}$:$Cr_{0.02}$ was observed in Figure S5, which is due to the low doping amount of Cr^{3+} (The molar feed ratio of Cr^{3+}: Ga^{3+} is 1%).[39] In the previous studies, the peak shift can be observed when increasing the doping amount of Cr^{3+} up to ∼20%, indicating the isomorphic substitution of smaller Cr^{3+} (ionic radius in VI coordination = 0.615 Å) for slightly bigger Ga^{3+} (ionic radius in VI coordination = 0.620 Å) in a $ZnGa_2O_4$ unit.[39] A similar conclusion was also confirmed in other documented reports.[14,40] In our case, since the radii of Cr^{3+} and Ge^{4+} ions (0.61 and 0.54 Å, respectively) are very close to that of the Ga^{3+} ion (0.62 Å), they are expected to substitute Ga^{3+} ions and occupy the octahedral sites.[22] To characterize the water dispersibility of ZGGO particles, we dispersed the as-prepared particles in an aqueous solution and measured the hydrodynamic particle size. As shown in Figure 1e, the dynamic light scattering (DLS) profile from aqueous solutions of these particles exhibits a single light scattering peak. The size distribution profile is rather symmetric, suggesting that there is no obvious population of larger particulates or aggregates. The particles after standing over 12 h can still be well dispersed in the aqueous solution (Figure S6a), which can further find support from the Tyndall effect upon green laser irradiation (Figure S6b). In addition, the particle surface ζ-potential changed −29.6 mV (Figure S6c). It is also found that the formed ZGGO particles can readily disperse in the molten NaCl even without stirring during the reaction, which is verified from the NIR persistent luminescence of ZGGO in the transparent NaCl crystal under UV light (inset of Figure 1e). This indicates there is no bulk or particle aggregation formed during the high temperature reaction, thus rendering as-prepared particles readily dispersible in the aqueous solution.

The chemical state of the prepared ZGGO particles is determined by the X-ray photoelectron spectroscopy (XPS), where peaks of O 1s, Zn 2p, Ga 2p, Ge 2p, and Cr 2p can be identified (Figures S7−S8). The high-resolution scanning of the Ga 2p, Ge 2p, and Cr 2p peaks is further presented in Figure 1f. The binding energies peaking at 1120.6 and 1222.7 eV can be ascribed to Ga $2p_{3/2}$ and Ge $2p_{3/2}$, respectively, with the corresponding fwhm of 1.45 and 1.61 eV, suggesting that the Ga and Ge atoms are bonded with O atoms with a single component (Ga $2p_{3/2}$ at 1118.0 eV for Ga_2O_3 and Ge $2p_{3/2}$ at 1220.2 eV for GeO_2) instead of being metallic clusters.[41] Furthermore, a main peak at 576.6 eV corresponds to Cr^{3+},[34,42] while the peaks for Cr^{5+}, Cr^{4+}, Cr^{2+}, and metallic Cr are not observed, suggesting that only Cr^{3+} exists in prepared particles, which is expected to replace Ga^{3+} ions.[43]

It is worth mentioning that the molten NaCl used here acts as a solvent for dissolving solid reactants and solvating ions by strong polarization and rapid movement of reactant species through convection and diffusion. This can not only offer an extremely inert high temperature environment for annealing but also render the reaction medium highly ionic. The latter can generally increase the contact area of reactants due to the

https://doi.org/10.1021/acs.jpcc.2c08045
J. Phys. Chem. C 2023, 127, 3733−3741

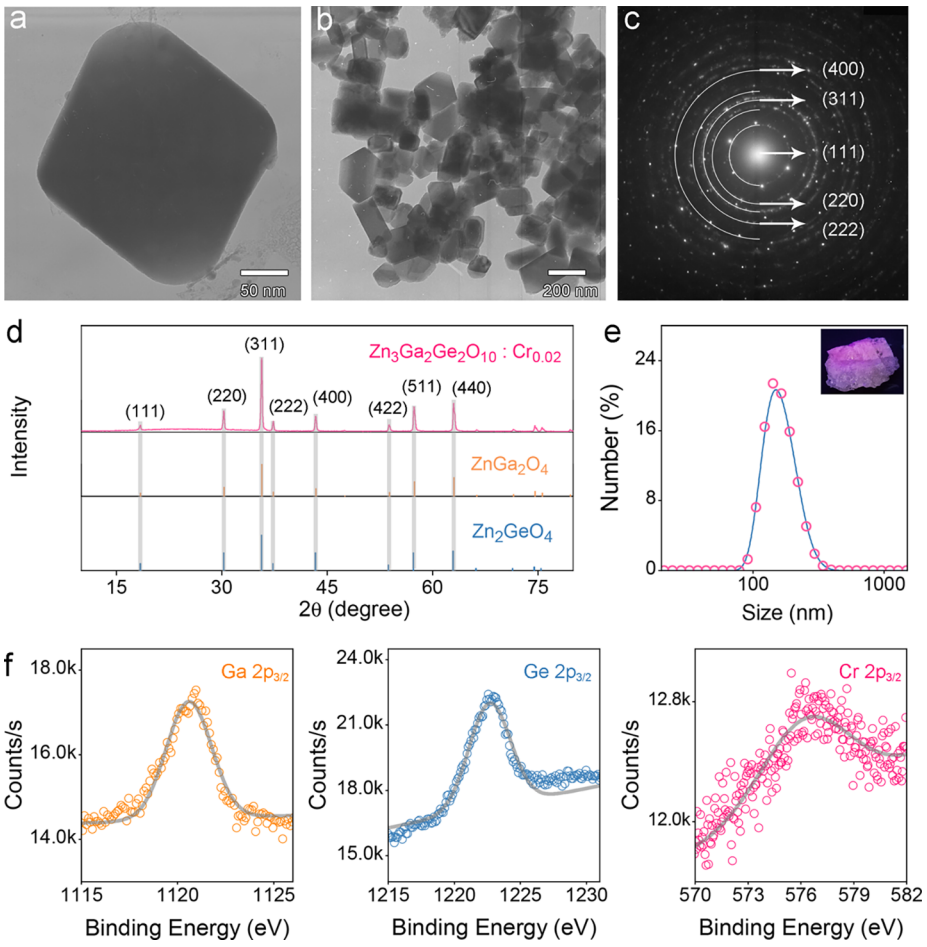

Figure 1. Representative TEM image (a), low magnification TEM image (b), selected area electron diffraction pattern with identified diffraction rings (c), powder X-ray diffraction patterns (d) together with JCPDS card data plotted at the bottom, hydrodynamic size distribution profile (e), and the XPS spectra for the Ga 2p, Ge 2p, and Cr 2p binding energy levels (f) of as-prepared ZGGO particles. The inset of (e) shows the digital photo of ZGGO embedded in the NaCl crystal under 254 nm UV excitation.

enhanced ionic mobility (diffusion rate on the order of 10^{-5}–10^{-8} cm^2 s^{-1}) and thereby provides strong columbic interactions among reactants, supporting the uniform growth of particles.[44,45] Furthermore, the molten NaCl is able to function as X-type (Lewis basic) ligands anchoring onto the particle surface and stabilizing the particles at high operating temperature, while the organic molecular surfactants cannot be utilized to modulate the morphology due to their thermal decomposition or oxidation. In principle, the mechanism of colloidal stabilization by molten NaCl is fundamentally different with the conventional electrostatic and steric repulsion between particles. The molten NaCl acting as a layer of surface-bound solvent ions can produce long-range charge-density oscillations around solute particles with a distance greatly exceeding the Debye screening length (~1 Å, $L_D = 1/\sqrt{4\pi\rho q^2/\varepsilon k_B T}$, where ρ is the ion concentration per unit volume, q is the unit charge, ε is the dielectric constant, and $k_B T$ is the thermal energy), which consequently decreases the probability that neighboring particles approach each other and aggregate.[32,46,47] In a control experiment without molten NaCl, the bulk ZGGO compound was obtained as expected through direct thermal treatment of the precursors (Figure S9), which were hardly dispersible in the aqueous solution. Some amorphous bulk aggregates were observed (Figure 2a) even after a super sonication treatment. Although solution-dispersible particles can be obtained through robust milling and strict size selection, these arduous postsynthesis procedures come at the expense of sacrificing optical properties and greatly reducing particle yield.[48] The observations from our control studies without molten NaCl confirm that molten NaCl participated in regulating the particle formation process.

In addition to the molten NaCl, citric acid is the other key factor in regulating the particle formation in the current strategy. As shown in Figure 2b, the resulting products are amorphous and aggregated in the absence of citric acid even though molten NaCl was used as the reaction medium. In comparison with ZGGO obtained with citric acid in Figure 1a, these ones without citric acid became aggregated and separated from the NaCl solvent (inset of Figure 2b), suggesting that the introduction of citric acid helps the particles to disperse in the NaCl solvent. Citric acid is a weak triprotic acid with three carboxylic acid moieties which can coordinate with metal ions and form a gel-like network structure (Figure 2c). In the presence of the organic matrix during the first stage of synthesis, the nucleation sites are evenly dispersed and numerous, ensuring a small crystallite size. In addition, the diffusion transport of particles in the network structure is limited, which thus offers a confined environment for the nucleation and growth of particles during high temperature

https://doi.org/10.1021/acs.jpcc.2c08045
J. Phys. Chem. C 2023, 127, 3733−3741

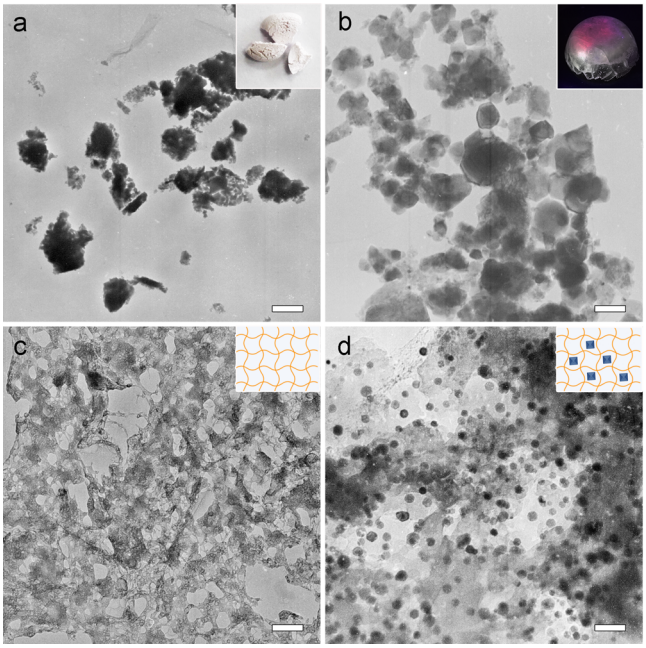

Figure 2. TEM images of ZGGO prepared in the absence of NaCl (a) and citric acid (b), respectively. The inset of (a) is the digital photo of the products, and the inset of (b) is the digital photo of the ZGGO embedded in the NaCl crystal under 254 nm UV excitation. TEM images of the network structure formed by chelating metal ions with citric acid (c) and followed by embedding NaCl into the three-dimensional network structure (d). The insets of c–d are the corresponding schematic structures. The embedded scale bars correspond to 500 nm.

heating. In our case of quaternary systems, another purpose of the citric acid-driven matrix is to ensure that the different metal precursors remain mixed evenly. Even in our system, ZGGO may not crystallize until >800 °C, long after the citric acid component has been decomposed. The homogeneity of the precursor can ensure that the reaction system remains amorphous until the final product begins to nucleate. It should be emphasized that there is no crystal formed during the formation stage of the network structure (Figure S10), and the line broadening in the XRD pattern of the dried powder may result from the disordered crystallites or glass substrate.[38] Thermogravimetric analysis of the network reveals a very sharp mass loss step around 200 °C (Figure S11), which is associated with a rapid, self-propagating combustion where citric acid acts as the oxidant and citrate acts as the organic fuel.[49] These results indicate that the presence of the complexation-associated network during the first stage of synthesis can ensure that nucleation sites are spatially confined and well-distributed, favoring for a controlled particle growth during the following stage. The introduction of NaCl into the three-dimensional network structure (Figure 2d) further controls the crystal growth and prevents the particles from aggregation, preferentially leading to particle formation with a well-defined morphology in the molten NaCl solution at temperatures above 800 °C.

The effect of NaCl on the persistent luminescence of as-prepared ZGGO particles is further investigated through steady-state and transient spectroscopy. Note that the ratio of citric acid to metal ions in the absence of NaCl is first optimized to be 1.5:1, so the effect of NaCl on the optical properties can be separated from the effects of citric acid (Figure S12). The excitation and emission spectra of ZGGO particles obtained in the absence of NaCl and citric acid are recorded at room temperature and provided in Figure 3a. Upon excitation at 260 nm, the particles exhibit an emission band in the red/NIR region from 600 to 850 nm due to the ^2E-$^4A_2$ transition of the distorted Cr^{3+} ions in the ZGGO host, originating from nonradiative energy transfer between the photoexcited host and the Cr^{3+} dopant.[50] As displayed in Figure S13, the luminescence emission shifts from the blue to red region upon the introduction of Cr^{3+} dopants. The emission band centered at 695 nm accounts for the deep red persistent luminescence of Cr^{3+} dopants.[34] The excitation spectrum monitored at 695 nm covers a broad spectral region (from 230 to 500 nm), where the dominant excitation peak at 260 nm can be attributed to the band-to-band transition of the ZGGO host, while the 407 nm excitation band originates from the inner $^4A_2$-$^4T_1$ transition of Cr^{3+} dopants (Figure S12).[21] The luminescent quantum yield for as-prepared ZGGO particles was determined to be ∼23.6%. In comparison with ZGGO obtained with NaCl, the emission profile (600 to 850 nm) of ZGGO particles obtained without NaCl in Figure 3b exhibits spectral broadening, with an increase of fwhm from 35.7 to 39.8 nm, and the excitation peak around 430 nm becomes the dominant feature of the excitation band. The broadening of the emission band of samples obtained without molten salt can be attributed to enhanced lattice strain, which is minimized in molten salts.[33,51] The narrowing of the emission peak which is important for enhancing color accuracy may originate from the narrowing of the particle size distribution and the larger crystal field splitting.[52] According to the fitting results of afterglow decay curves, the particles obtained with molten salt have an average decay lifetime of the persistent luminescence centered at 695 nm up to 486.7 s, 10 times longer than that of particles obtained without NaCl (only around 40 s), regardless of the molar ratios of citric acid to total metal ions from 0:1 to 3:1 (Figure 3c and Figure S14), which is similar to the previously documented report.[2] In contrast, the lifetime of the slow decay component of the former samples is up to 609.3 s, an order of magnitude higher than that (53.9 s) of the latter samples (Table S1). These results confirm that the current molten salt synthesis is able to resist antisite defects in ZGGO particles, which is essential for the generation of persistent luminescence from its Cr-doped counterparts.

Despite having a relatively low doping concentration, when Cr^{3+} ions replace the position of Ga^{3+}, a 3D array of corner sharing tetrahedra reformed, which is expected to affect the magnetic behavior for ZGGO particles due to the presence of isotropic spin Cr^{3+} (d^3).[53] To probe this effect, the magnetic properties of as-prepared ZGGO particles are further investigated using a VSM at room temperature. The results shown in Figure 3d reveal that all ZGGO particles, regardless of the involvement of NaCl, display typical hysteresis loops indicative of ferromagnetism and exhibit obvious magnetic anisotropy, suggesting that as-prepared ZGGO particles exhibit ferromagnetism. Interestingly, the particles prepared in the molten NaCl solution show significantly higher saturation magnetization (M_s) than those formed in the absence of NaCl (0.108 vs. 0.018 emu/g), likely due to the morphology control of particles in the presence of the molten salt. Furthermore, typically 2 min were long enough to completely collect the particles dispersed in water when exerting a permanent magnetic field of 0.5 T (inset of Figure 3d). As

https://doi.org/10.1021/acs.jpcc.2c08045
J. Phys. Chem. C 2023, 127, 3733−3741

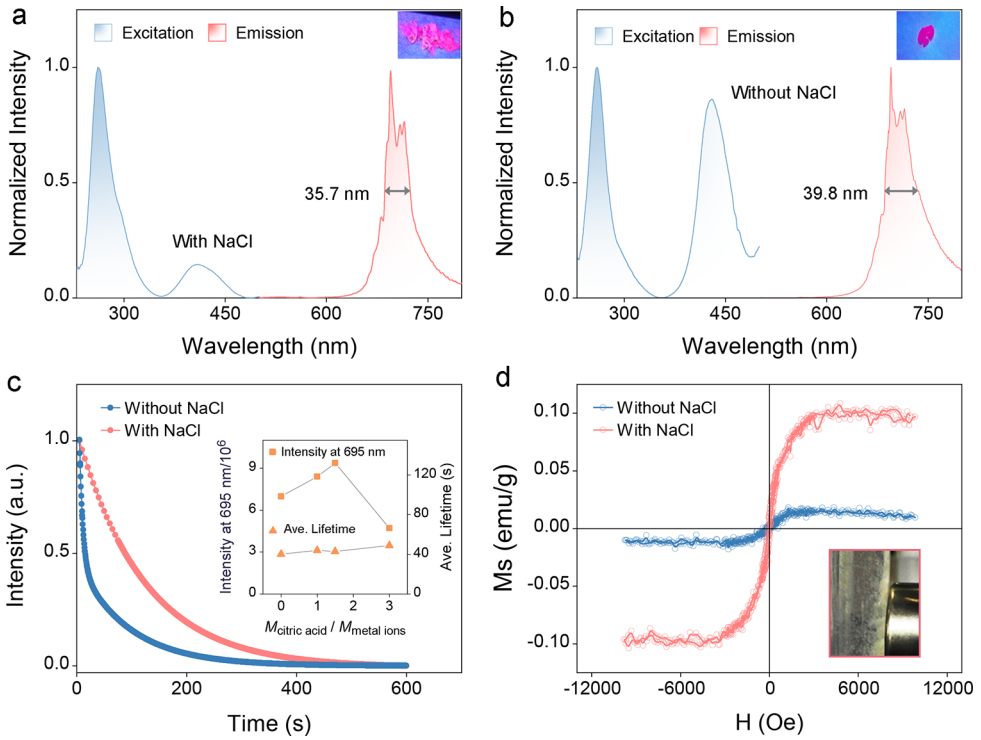

Figure 3. Excitation and emission spectra of ZGGO particles prepared with NaCl (a) and without NaCl (b) with a molar ratio of citric acid to total metal ions of 1.5:1. (The insets show the digital photo of ZGGO particles under irradiation with 254 nm UV light.) Together with the corresponding NIR persistent luminescence decay curves after a 5 min excitation at 261 nm (c), the inset of (c) shows the photoluminescence intensity at 695 nm and average decay lifetime of ZGGO particles prepared with different molar ratios of citric acid to total metal ions (0:1, 1:1, 1.5:1, and 3:1) in the absence of NaCl. Room-temperature magnetization curves (d) of ZGGO samples formed with or without NaCl. Inset: image of an aqueous dispersion of ZGGO particles formed with NaCl after being placed close to a magnet (0.5 T) for 2 min. The white ZGGO particles can be separated and aggregated by an external magnetic field from their homogeneous dispersion in the water solution.

aforementioned, the ZGGO particles obtained with NaCl were around 114.5 nm with cube- and quasicube-like shapes, while their bulk counterpart was obtained in the absence of NaCl. The lattice parameters of oxide particles were generally found to be higher than those of the corresponding bulk forms.[54] According to the XRD results, the ZGGO particle prepared with NaCl has a cubic structure with a calculated lattice parameter of a = 8.3834 Å, slightly larger than that (8.3443 Å) of the bulk sample prepared without NaCl. This is also in agreement with a previous report where the lattice expands in oxide particles.[55] The increase in the lattice parameter with a decreasing particle size may result from the oxygen vacancy associated with particles.[54,56] Actually, the room-temperature ferromagnetism has been observed previously in nonmagnetic metal oxide particles such as CeO_2, Al_2O_3, ZnO, In_2O_3, SnO_2, etc.,[56−58] originating from the oxygen vacancies on the particle surface due to exchange interactions among localized electron spin moments, and the electrons trapped in oxygen vacancies (F center) are polarized to give room-temperature ferromagnetism.[54] The oxygen defects of ZGGO particles obtained in NaCl can be determined from the XPS spectra for the O 1s signal (Figure S15).[59] Generally, such defect-induced ferromagnetism was often reduced upon high-temperature annealing of the as-synthesized particles as a result of structural ordering, which leads to the reduction in the surface oxygen vacancy concentration.[60] Therefore, it seems that a high temperature calcination is detrimental to the ferromagnetism of metal oxide particles. Surprisingly, the ZGGO particles in our current strategy directly produced in the molten NaCl solution not only maintain the ferromagnetism properties but also possess an enhanced M_s, 6 times higher than that of particles obtained without NaCl. These findings provide a new strategy to further study the magnetic properties of other metal oxides.

CONCLUSIONS

In summary, water-dispersible and persistent luminescent ZGGO particles were directly obtained with a well-defined cubic morphology through a one-step molten salt synthesis approach in combination with citric acid. It was demonstrated that citric acid binding with metal ions can form a complexation-associated network during the first stage of synthesis, which creates a confined environment for achieving a small crystallite size and limiting particle diffusion during high temperature heating. Meanwhile, using molten NaCl as the reaction medium not only provides strong columbic interactions among reactants that favor uniform particle growth but also effectively suppresses particle aggregation through the formation of a robust ionic solvation shell around the particles. Benefiting from the synergistic effects of these two factors on the particle nucleation and growth process, the persistent luminescence decay lifetime of ZGGO particles was improved by a factor of 10 compared with those obtained without NaCl. Together with the enhanced ferromagnetism properties, the multifunctional ZGGO particles may be used in multiple optical/magnetic fields. The proposed molten salt synthesis strategy offers a reliable in situ approach for directly obtaining water-dispersible and highly persistent luminescent

https://doi.org/10.1021/acs.jpcc.2c08045
J. Phys. Chem. C 2023, 127, 3733−3741

particles in a controlled manner and may inform the synthesis of other complex metal oxide particles in the future.

■ ASSOCIATED CONTENT

Supporting Information

The Supporting Information is available free of charge at https://pubs.acs.org/doi/10.1021/acs.jpcc.2c08045.

Images of experimental installation; reactions involved at different synthesis stages; images of mixed precursor solutions; low magnification TEM image and particle size histogram; digital photos of aqueous dispersion of prepared ZGGO particles and their zeta potential profile; XPS pattern and X-ray diffraction pattern of ZGGO; powder X-ray diffraction pattern and thermogravimetric curve of network structure formed by chelating metal ions with citric acid; excitation and emission spectra; NIR persistent luminescence decay curves of ZGGO particles prepared with different molar ratios of citric acid to total metal ions in the absence of NaCl; XPS spectra for O 1s signal of ZGGO particles; and parameters for multiexponential fits of luminescence decay curves of different ZGGO particles (PDF)

■ AUTHOR INFORMATION

Corresponding Authors

Lihong Jing − *Key Laboratory of Colloid, Interface and Chemical Thermodynamics, Institute of Chemistry, Chinese Academy of Sciences, Beijing 100190, China;* orcid.org/0000-0001-6115-2743; Phone: +86 10 6256 2821; Email: jinglh@iccas.ac.cn

Mingyuan Gao − *Key Laboratory of Colloid, Interface and Chemical Thermodynamics, Institute of Chemistry, Chinese Academy of Sciences, Beijing 100190, China; State Key Laboratory of Radiation Medicine and Protection, School for Radiological and Interdisciplinary Sciences (RAD-X) and Collaborative Innovation Center of Radiation Medicine of Jiangsu Higher Education Institutions, Soochow University, Suzhou 215123, China*; Email: gaomy@iccas.ac.cn

Authors

Xiaojun Wei − *Key Laboratory of Colloid, Interface and Chemical Thermodynamics, Institute of Chemistry, Chinese Academy of Sciences, Beijing 100190, China;* Present Address: Department of Chemical Engineering, University of South Carolina, Columbia, SC 29208, USA; orcid.org/0000-0002-6229-6228

Haoran Ning − *Key Laboratory of Colloid, Interface and Chemical Thermodynamics, Institute of Chemistry, Chinese Academy of Sciences, Beijing 100190, China*

Xiaodan Huang − *Key Laboratory of Colloid, Interface and Chemical Thermodynamics, Institute of Chemistry, Chinese Academy of Sciences, Beijing 100190, China*

Collin F. Perkinson − *Department of Chemistry, Massachusetts Institute of Technology, Cambridge, Massachusetts 02139, United States;* orcid.org/0000-0002-5676-1998

Chunyan Liu − *Key Laboratory of Colloid, Interface and Chemical Thermodynamics, Institute of Chemistry, Chinese Academy of Sciences, Beijing 100190, China*

Zhuoyao Dong − *Key Laboratory of Colloid, Interface and Chemical Thermodynamics, Institute of Chemistry, Chinese Academy of Sciences, Beijing 100190, China*

Complete contact information is available at: https://pubs.acs.org/10.1021/acs.jpcc.2c08045

Notes

The authors declare no competing financial interest.

■ ACKNOWLEDGMENTS

The authors acknowledge financial support from the National Natural Science Foundation of China (NSFC, 22177115, 81671755, 81720108024), the National Key Research and Development Program of China (2018YFA0208800), the Youth Innovation Promotion Association CAS (2018042), and the State Key Laboratory of Luminescence and Applications (SKLA-2019-01).

■ REFERENCES

(1) Wei, X.; Huang, X.; Zeng, Y.; Jing, L.; Tang, W.; Li, X.; Ning, H.; Sun, X.; Yi, Y.; Gao, M. Longer and Stronger: Improving Persistent Luminescence in Size-Tuned Zinc Gallate Nanoparticles by Alcohol-Mediated Chromium Doping. *ACS Nano* **2020**, *14*, 12113−12124.

(2) Abdukayum, A.; Chen, J.-T.; Zhao, Q.; Yan, X.-P. Functional near infrared-emitting Cr^{3+}/Pr^{3+} co-doped zinc gallogermanate persistent luminescent nanoparticles with superlong afterglow for in vivo targeted bioimaging. *J. Am. Chem. Soc.* **2013**, *135*, 14125−14133.

(3) Sun, S.-K.; Wang, H.-F.; Yan, X.-P. Engineering persistent luminescence nanoparticles for biological applications: from biosensing/bioimaging to theranostics. *Acc. Chem. Res.* **2018**, *51*, 1131−1143.

(4) Huang, K.; Le, N.; Wang, J. S.; Huang, L.; Zeng, L.; Xu, W. C.; Li, Z.; Li, Y.; Han, G. Designing next generation of persistent luminescence: recent advances in uniform persistent luminescence nanoparticles. *Adv. Mater.* **2022**, *34*, 2107962.

(5) Allix, M.; Chenu, S.; Véron, E.; Poumeyrol, T.; Kouadri-Boudjelthia, E. A.; Alahrache, S.; Porcher, F.; Massiot, D.; Fayon, F. Considerable improvement of long-persistent luminescence in germanium and tin substituted $ZnGa_2O_4$. *Chem. Mater.* **2013**, *25*, 1600−1606.

(6) Li, X.; Yin, C.; Liew, S. S.; Lee, C.-S.; Pu, K. Organic Semiconducting Luminophores for Near-Infrared Afterglow, Chemiluminescence, and Bioluminescence Imaging. *Adv. Funct. Mater.* **2021**, *31*, 2106154.

(7) Ji, C.; Tan, J.; Yuan, Q. Defect Luminescence Based Persistent Phosphors—From Controlled Synthesis to Bioapplications. *Chin. J. Chem.* **2021**, *39*, 3188−3198.

(8) Liu, X.; Ji, Q.; Hu, Q.; Li, C.; Chen, M.; Sun, J.; Wang, Y.; Sun, Q.; Geng, B. Dual-mode long-lived luminescence of Mn^{2+}-doped nanoparticles for multilevel anticounterfeiting. *ACS Appl. Mater. Interfaces* **2019**, *11*, 30146−30153.

(9) Maldiney, T.; Bessière, A.; Seguin, J.; Teston, E.; Sharma, S. K.; Viana, B.; Bos, A. J.; Dorenbos, P.; Bessodes, M.; Gourier, D. The in vivo activation of persistent nanophosphors for optical imaging of vascularization, tumours and grafted cells. *Nat. Mater.* **2014**, *13*, 418−426.

(10) Wang, J.; Ma, Q.; Zheng, W.; Liu, H.; Yin, C.; Wang, F.; Chen, X.; Yuan, Q.; Tan, W. One-dimensional luminous nanorods featuring tunable persistent luminescence for autofluorescence-free biosensing. *ACS Nano* **2017**, *11*, 8185−8191.

(11) Liang, L.; Chen, N.; Jia, Y.; Ma, Q.; Wang, J.; Yuan, Q.; Tan, W. Recent progress in engineering near-infrared persistent luminescence nanoprobes for time-resolved biosensing/bioimaging. *Nano Res.* **2019**, *12*, 1279−1292.

(12) Zhuang, Y.; Wang, L.; Lv, Y.; Zhou, T. L.; Xie, R. J. Optical data storage and multicolor emission readout on flexible films using deep-trap persistent luminescence materials. *Adv. Funct. Mater.* **2018**, *28*, 1705769.

(13) Li, Z.; Wang, Q.; Wang, Y.; Ma, Q.; Wang, J.; Li, Z.; Li, Y.; Lv, X.; Wei, W.; Chen, L. Background-free latent fingerprint imaging

based on nanocrystals with long-lived luminescence and pH-guided recognition. *Nano Res.* **2018**, *11*, 6167−6176.
(14) Zhou, Z.; Zheng, W.; Kong, J.; Liu, Y.; Huang, P.; Zhou, S.; Chen, Z.; Shi, J.; Chen, X. Rechargeable and LED-activated $ZnGa_2O_4$: Cr^{3+} near-infrared persistent luminescence nanoprobes for background-free biodetection. *Nanoscale* **2017**, *9*, 6846−6853.
(15) Yen, W. M.; Yamamoto, H. *Practical applications of phosphors*; CRC Press: 2018; 528pp, eBook ISBN9781315219974, DOI: 10.1201/9781315219974.
(16) Wang, J.; Ma, Q.; Wang, Y.; Shen, H.; Yuan, Q. Recent progress in biomedical applications of persistent luminescence nanoparticles. *Nanoscale* **2017**, *9*, 6204−6218.
(17) Sun, X.; Song, L.; Liu, N.; Shi, J.; Zhang, Y. Chromium-Doped Zinc Gallate Near-Infrared Persistent Luminescence Nanoparticles in Autofluorescence-Free Biosensing and Bioimaging: A Review. *ACS Applied Nano Materials* **2021**, *4*, 6497−6514.
(18) Li, Z.; Zhang, Y.; Wu, X.; Huang, L.; Li, D.; Fan, W.; Han, G. Direct Aqueous-Phase Synthesis of Sub-10 nm "Luminous Pearls" with Enhanced in Vivo Renewable Near-Infrared Persistent Luminescence. *J. Am. Chem. Soc.* **2015**, *137*, 5304−5307.
(19) Wang, J.; Ma, Q.; Hu, X.-X.; Liu, H.; Zheng, W.; Chen, X.; Yuan, Q.; Tan, W. Autofluorescence-free targeted tumor imaging based on luminous nanoparticles with composition-dependent size and persistent luminescence. *ACS Nano* **2017**, *11*, 8010−8017.
(20) Fu, L.; Wang, J.; Chen, N.; Ma, Q.; Lu, D.; Yuan, Q. Enhancement of long-lived luminescence in nanophosphors by surface defect passivation. *Chem. Commun.* **2020**, *56*, 6660−6663.
(21) Srivastava, B. B.; Kuang, A.; Mao, Y. Persistent luminescent sub-10 nm Cr doped $ZnGa_2O_4$ nanoparticles by a biphasic synthesis route. *Chem. Commun.* **2015**, *51*, 7372−7375.
(22) Yang, J.; Liu, Y.; Zhao, Y.; Gong, Z.; Zhang, M.; Yan, D.; Zhu, H.; Liu, C.; Xu, C.; Zhang, H. Ratiometric afterglow nanothermometer for simultaneous in situ bioimaging and local tissue temperature sensing. *Chem. Mater.* **2017**, *29*, 8119−8131.
(23) Basavaraju, N.; Priolkar, K. R.; Gourier, D.; Bessière, A.; Viana, B. Order and disorder around Cr^{3+} in chromium doped persistent luminescent AB_2O_4 spinels. *Phys. Chem. Chem. Phys.* **2015**, *17*, 10993−10999.
(24) Abdurahman, R.; Yang, C.-X.; Yan, X.-P. Conjugation of a Photosensitizer to near infrared light renewable persistent luminescence nanoparticles for photodynamic therapy. *Chem. Commun.* **2016**, *52*, 13303−13306.
(25) Srivastava, B. B.; Gupta, S. K.; Mohan, S.; Mao, Y. Molten-Salt-Assisted Annealing for Making Colloidal $ZnGa_2O_4$: Cr Nanocrystals with High Persistent Luminescence. *Chem.—Eur. J.* **2021**, *27*, 11398−11405.
(26) Wang, J.; Li, J.; Yu, J.; Zhang, H.; Zhang, B. Large hollow cavity luminous nanoparticles with near-infrared persistent luminescence and tunable sizes for tumor afterglow imaging and chemo-/photodynamic therapies. *ACS Nano* **2018**, *12*, 4246−4258.
(27) Shi, J.; Sun, X.; Li, J.; Man, H.; Shen, J.; Yu, Y.; Zhang, H. Multifunctional near infrared-emitting long-persistence luminescent nanoprobes for drug delivery and targeted tumor imaging. *Biomaterials.* **2015**, *37*, 260−270.
(28) Zou, R.; Huang, J.; Shi, J.; Huang, L.; Zhang, X.; Wong, K.-L.; Zhang, H.; Jin, D.; Wang, J.; Su, Q. Silica shell-assisted synthetic route for mono-disperse persistent nanophosphors with enhanced in vivo recharged near-infrared persistent luminescence. *Nano Res.* **2017**, *10*, 2070−2082.
(29) Mao, Y.; Park, T.-J.; Zhang, F.; Zhou, H.; Wong, S. S. Environmentally Friendly Methodologies of Nanostructure Synthesis. *Small* **2007**, *3*, 1122−1139.
(30) Mao, Y.; Tran, T.; Guo, X.; Huang, J. Y.; Shih, C. K.; Wang, K. L.; Chang, J. P. Luminescence of Nanocrystalline Erbium-Doped Yttria. *Adv. Funct. Mater.* **2009**, *19*, 748−754.
(31) Gupta, S. K.; Mao, Y. Recent developments on molten salt synthesis of inorganic nanomaterials: A review. *J. Phys. Chem. C* **2021**, *125*, 6508−6533.
(32) Liu, X.; Fechler, N.; Antonietti, M. Salt melt synthesis of ceramics, semiconductors and carbon nanostructures. *Chem. Soc. Rev.* **2013**, *42*, 8237−8265.
(33) Srivastava, V.; Kamysbayev, V.; Hong, L.; Dunietz, E.; Klie, R. F.; Talapin, D. V. Colloidal chemistry in molten salts: Synthesis of luminescent $In_{1-x}Ga_xP$ and $In_{1-x}Ga_xAs$ quantum dots. *J. Am. Chem. Soc.* **2018**, *140*, 12144−12151.
(34) Wei, X.; Kershaw, S. V.; Huang, X.; Jiao, M.; Beh, C. C.; Liu, C.; Sarmadi, M.; Rogach, A. L.; Jing, L. Continuous Flow Synthesis of Persistent Luminescent Chromium-Doped Zinc Gallate Nanoparticles. *J. Phys. Chem. Lett.* **2021**, *12*, 7067−7075.
(35) Huang, X.; Wei, X.; Zeng, Y.; Jing, L.; Ning, H.; Sun, X.; Li, Y.; Li, D.; Yi, Y.; Gao, M. Turning-on persistent luminescence out of chromium-doped zinc aluminate nanoparticles by instilling antisite defects under mild conditions. *Nanoscale* **2021**, *13*, 8514−8523.
(36) Danks, A. E.; Hall, S. R.; Schnepp, Z. The evolution of 'sol-gel'chemistry as a technique for materials synthesis. *Materials Horizons* **2016**, *3*, 91−112.
(37) Vaqueiro, P.; López-Quintela, M. A. Influence of Complexing Agents and pH on Yttrium-Iron Garnet Synthesized by the Sol-Gel Method. *Chem. Mater.* **1997**, *9*, 2836−2841.
(38) da Silva, M. N.; de Carvalho, J. M.; de Abreu Fantini, M. C.; Chiavacci, L. A.; Bourgaux, C. Nanosized $ZnGa_2O_4$: Cr^{3+} spinels as highly luminescent materials for bioimaging. *ACS Applied Nano Materials* **2019**, *2*, 6918−6927.
(39) Arroyo, E.; Medrán, B.; Castaing, V.; Lozano, G.; Ocaña, M.; Becerro, A. I. Persistent luminescence of transparent $ZnGa_2O_4$: Cr^{3+} thin films from colloidal nanoparticles of tunable size. *J. Mater. Chem. C* **2021**, *9*, 4474−4485.
(40) Bessière, A. l.; Sharma, S. K.; Basavaraju, N.; Priolkar, K. R.; Binet, L.; Viana, B.; Bos, A. J.; Maldiney, T.; Richard, C.; Scherman, D. Storage of visible light for long-lasting phosphorescence in chromium-doped zinc gallate. *Chem. Mater.* **2014**, *26*, 1365−1373.
(41) Can, M. M.; Jaffari, G. H.; Aksoy, S.; Shah, S. I.; Fırat, T. Synthesis and characterization of $ZnGa_2O_4$ particles prepared by solid state reaction. *J. Alloy. Compd.* **2013**, *549*, 303−307.
(42) Galtayries, A.; Warocquier-Clérout, R.; Nagel, M. D.; Marcus, P. Fibronectin adsorption on Fe-Cr alloy studied by XPS. *Surf. Interface Anal.* **2006**, *38*, 186−190.
(43) Guo, D.; Wu, Z.; Li, P.; Wang, Q.; Lei, M.; Li, L.; Tang, W. Magnetic Anisotropy and Deep Ultraviolet Photoresponse Characteristics in Ga_2O_3:Cr Vermicular Nanowire Thin Film Nanostructure. *RSC Adv.* **2015**, *5*, 12894−12898.
(44) Gonell, F.; Sanchez-Sanchez, C. M.; Vivier, V.; Laberty-Robert, C.; Portehault, D. Experimental Descriptors for the Synthesis of Multicationic Nickel Perovskite Nanoparticles for Oxygen Reduction. *ACS Appl. Nano Mater.* **2020**, *3*, 7482−7489.
(45) Jiang, D.; Wang, X.; Chen, R.; Sun, J.; Kang, H.; Ji, D.; Liu, Y.; Wei, D. Self-Expanding Molten Salt-Driven Growth of Patterned Transition-Metal Dichalcogenide Crystals. *J. Am. Chem. Soc.* **2022**, *144*, 8746−8755.
(46) Zhang, H.; Dasbiswas, K.; Ludwig, N. B.; Han, G.; Lee, B.; Vaikuntanathan, S.; Talapin, D. V. Stable colloids in molten inorganic salts. *Nature* **2017**, *542*, 328−331.
(47) Kamysbayev, V.; Srivastava, V.; Ludwig, N. B.; Borkiewicz, O. J.; Zhang, H.; Ilavsky, J.; Lee, B.; Chapman, K. W.; Vaikuntanathan, S.; Talapin, D. V. Nanocrystals in molten salts and ionic liquids: experimental observation of ionic correlations extending beyond the Debye length. *ACS Nano* **2019**, *13*, 5760−5770.
(48) le Masne De Chermont, Q.; Chanéac, C.; Seguin, J.; Pellé, F.; Maîtrejean, S.; Jolivet, J.-P.; Gourier, D.; Bessodes, M.; Scherman, D. Nanoprobes with near-infrared persistent luminescence for in vivo imaging. *Proc. Nat. Acad. Sci.* **2007**, *104*, 9266−9271.
(49) Wen, W.; Wu, J. M. Nanomaterials via Solution Combustion Synthesis: a Step Nearer to Controllability. *RSC Adv.* **2014**, *4*, 58090−58100.
(50) Pan, Z.; Lu, Y.-Y.; Liu, F. Sunlight-activated long-persistent luminescence in the near-infrared from Cr^{3+}-doped zinc gallogermanates. *Nat. Mater.* **2012**, *11*, 58−63.

(51) Srivastava, V.; Liu, W.; Janke, E. M.; Kamysbayev, V.; Filatov, A. S.; Sun, C.-J.; Lee, B.; Rajh, T.; Schaller, R. D.; Talapin, D. V. Understanding and curing structural defects in colloidal gaas nanocrystals. *Nano Lett.* **2017**, *17*, 2094−2101.
(52) Bai, Q.; Zhao, S.; Xu, Z.; Li, P. Tunable luminescence in co-doped $Zn_3Al_2Ge_2O_{10}$: Cr^{3+} by controlling crystal field splitting and nephelauxetic effect. *J. Rare Earth.* **2020**, *38*, 1265−1272.
(53) Dutton, S. E.; Huang, Q.; Tchernyshyov, O.; Broholm, C.; Cava, R. J. Sensitivity of the magnetic properties of the $ZnCr_2O_4$ and $MgCr_2O_4$ spinels to nonstoichiometry. *Phys. Rev. B* **2011**, *83*, 064407.
(54) Sundaresan, A.; Bhargavi, R.; Rangarajan, N.; Siddesh, U.; Rao, C. Ferromagnetism as a universal feature of nanoparticles of the otherwise nonmagnetic oxides. *Phys. Rev. B* **2006**, *74*, 161306.
(55) Tsunekawa, S.; Ishikawa, K.; Li, Z.-Q.; Kawazoe, Y.; Kasuya, A. Origin of anomalous lattice expansion in oxide nanoparticles. *Phys. Rev. Lett.* **2000**, *85*, 3440.
(56) Ogale, S. B. Dilute doping, defects, and ferromagnetism in metal oxide systems. *Adv. Mater.* **2010**, *22*, 3125−3155.
(57) Kamble, V. B.; Umarji, A. M. Correlating defect induced ferromagnetism and gas sensing properties of undoped tin oxide sensors. *Appl. Phys. Lett.* **2014**, *104*, 251912.
(58) Venkatesan, M.; Fitzgerald, C.; Coey, J. M. D. Unexpected magnetism in a dielectric oxide. *Nature* **2004**, *430*, 630−630.
(59) Wang, R.; van Dorp, L.; Shaw, L. P.; Bradley, P.; Wang, Q.; Wang, X.; Jin, L.; Zhang, Q.; Liu, Y.; Rieux, A.; et al. The global distribution and spread of the mobilized colistin resistance gene mcr-1. *Nat. Commun.* **2018**, *9*, 1179.
(60) Kamble, V. B.; Bhat, S.; Umarji, A. Investigating thermal stability of structural defects and its effect on d0 ferromagnetism in undoped SnO_2. *J. Appl. Phys.* **2013**, *113*, 244307.

https://doi.org/10.1021/acs.jpcc.2c08045
J. Phys. Chem. C 2023, 127, 3733−3741